

## **Does SW monsoon influence suspended particulate matter flux into the Arabian Sea?**

**Bangalore. R. Raghavan<sup>†</sup> and Onkar. S. Chauhan<sup>‡</sup>**

<sup>†</sup>Department of Marine Geology, Mangalore University, Mangalore, India-574199  
ragvon@yahoo.com

<sup>‡</sup>National Institute of Oceanography CSIR, Dona Paula, Goa, 403004-India  
onkar@nio.org

---

**ABSTRACT:** Seasonal enhancement in the flux of suspended particulate matter (TSM) has been attributed to the climatology of the southwest monsoon (SWM) in time series trap experiment in the Arabian Sea. To determine the influence of climate on TSM influx, we have obtained and evaluated synoptic variations in TSM, during the SWM, the pre and the post monsoon seasons over the continental margin of the SE Arabian Sea during 2007. We found high TSM during the SWM ( $> 82 \text{ mg l}^{-1}$ ) over the entire inner shelf. Contrary to the distribution over the inner shelf, there occurs uniformly low TSM ( $12\text{-}24 \text{ mg l}^{-1}$ ) over the entire outer-shelf (water depth  $> 30 \text{ m}$ ) round the year. We, therefore, propose that higher fluvial influx during SWM do not necessarily enhance supply of suspended particulate matter into the offshore regions of the SE Arabian Sea.

**ADDITIONAL INDEX WORDS:** SW monsoon, suspended particulate matter, SE Arabian Sea, morphodynamics

---

### **INTRODUCTION**

Climate plays an important role for yield, influx and dispersal pathways of suspended particulate matter (TSM) into marine environment (Weaver, 1989; Chauhan et al., 2006; Naqvi et al., 2009; Rixen et al., 2009 and references therein). The role of climate on suspended particulate matter influx into the Arabian Sea has been evaluated under trap experiment (with three trap moorings at the central, the eastern and the western region; Nair et al., 1989; Haake et al., 1993; 1996; Rixen et al., 2009). These studies have reported an enhanced supply of particulate matter into the entire Arabian Sea during the southwest monsoon (SWM). The prevalence of an intense rainfall, an augmented fluvial flux, the vigorous winds, and upwelling coupled biogeochemical processes (Nair et al., 1989; Haake et al., 1993; 1996; Nair et al., 1999) were found to enhance the flux of TSM into the deeper regions of the Arabian Sea. Because the TSM flux was persistent only during the SWM, role of hydrodynamic processes was considered insignificant (Nair et al., 1989; Haake et al., 1993; Rixen et al., 2009 and references therein). These inferences suggested that during the peak

precipitation time (SWM) associated with the high fluvial flux, offshore supply of the TSM should enhance.

The Indian Remote Sensing Satellite (IRS P-4) provides high resolution synoptic view of suspended particulate matter distribution with 2 days repeativity. The SW continental margin along the eastern Arabian Sea (average precipitation  $\sim 2700$  mm year<sup>-1</sup>) is ideal for evaluating the influence of an intense SWM precipitation regime over TSM supply because it has a network of high gradient rivers which are fed by a high precipitation during the SWM (Chauhan and Gujar, 1996; Chauhan et al., 2010a&b). We present the measured and the imagery derived seasonal TSM patterns and the variations in current regime to decipher processes that regulate dispersal and sink pathways of TSM over the SW continental margin of the India. Our study also reevaluates if TSM content in the offshore waters increases during the SWM, as is the case in the traps of the Arabian Sea (Nair et al., 1989; Haake et al., 1993; Nair et al., 1999), when the fluvial influx is at its maximum.

## **STUDY AREA**

The SW continental margin of India is found suitable because it has a regional physiographic high along the west coast, and unlike the northern region of the Arabian Sea it receives about 2700 mm rainfall during the SWM (June – September; Chauhan et al. 2011a). The area is therefore expected to have a high fluvial influx through a network of local rivers. We have chosen the central region of this area. The area is a hub of neo-urbanization due to setting up of a naval base and an atomic plant. The region has a tropical humid climate which is supportive of an intense chemical weathering regime (Chauhan et al. 2010b; Chauhan et al., 2010b (this reference is added into the cited literature). Associated with the reversal of winds due to the prevalence of monsoon, there is a marked seasonality in the regional hydrography (Fig.1). During the SWM, the Indian Monsoon Current (also known as West Indian Current) carries high salinity the Arabian Sea Water into the Bay of Bengal through equatorwards hydrography (Vinayachandran et al., 1999). After the SWM, the polewards hydrography (the East India Coastal Current) prevails in the study area (Kumar et al., 2004 and references therein). The study area therefore has a alongshore hydrography round the year.

## **METHODOLOGY**

In order to resolve the influence of the SWM, midtide-synchronous field measurements were carried out between 13.30 – 15.15<sup>0</sup>N; 73.30 – 74.30<sup>0</sup>E) at predetermined 24 stations spreading across the study area during 24<sup>th</sup> March- 4<sup>th</sup> April, (pre SWM) 23<sup>rd</sup> July- 6<sup>th</sup> August (SWM) and 29<sup>th</sup> November- 11<sup>th</sup> December of 2007 (post SWM). One liter of sea water was collected in polyurethane

sterile bottles, and was filtered using a Millipore filtration system. TSM had been estimated as per the protocol of JGOFS (matter retained on  $<0.45 \mu\text{m}$  optipure fiber filter paper; UNESCO, 1994). The position of each of the sampling stations was determined using a differential GPS system.

Besides, a finer resolution regional variation in TSM distributions had been obtained also from IRS-P4 OCM- data for path-09 row-13 (spectral channel central wavelength (bandwidth): 412(20), 443(20), 490(20), 510(20), 555(20), 670(20), 780(40), 860(40) nm; spatial resolution: 0.36 km; payload altitude: 760 km; satellite overpass:  $1200 \pm 0020$  hrs local standard time). We have processed over 110 images. The algorithm of Tassan (1994) is area specific and is found to have limitations in case II waters. Being specific to TSM deficient waters, it has upper detection limits of  $4 \text{ mg l}^{-1}$ . The Indian coast line has several major and minor rivers, and these discharge a large amount of suspended particulate matter into the sea. Considering the area specific needs, the Space Application Center (SAC) of the Indian Space Research Organization, upon the launch of IRS OCM-4, has undertaken a calibration and a validation programme to develop a dedicated algorithm for IRS P-4 OCM products for the Indian Coastal waters (for details refer Prasad et al., 2002; SAC report, 2004). In the present study, the OCM data were analyzed as per the specific protocol of SAC (2004) applying the atmospheric correction and bio-optical algorithms developed initially for IRS-P-3 MOS data (Mohan et al., 1998) and later modified for IRS-P4 OCM data (Chauhan et al. 2002).

Following the said protocol, each image was provided with atmospheric, aerosol, and geometric corrections (Chauhan et al 2002; SAC report 2000, 2004; Prasad et al., 2002;). The detail of procedures used for the atmospheric, aerosol, cloud corrections etc. are described below (SAC Report, 2004):

### **Geometric correction**

Validation of images and derivation of regional synoptic patterns from imageries require careful geometric correction and co-registration of the successive images within an error limit of one pixel. For which a two-stage approach has been followed. (SAC reports 2000, 2004; Prasad et al. 2002). On each imagery, geometric correction was applied to remove image distortion and to bring a standard geographic projection, with modified everest datum (i.e., a local geodetic datum, based on the everest spheroid that best fits the extent of the Indian subcontinent). Subsequently, co-registration had been done by warping one image to the other using polynomial transformation. The transformation was done by matching more than 25 pairs of Ground Control Points (GCP) on the images. The re-sampling at both the stages was performed by cubic convolution interpolation

techniques to keep the spatial distortions at a minimum (Legeckis and Pitchard 1976; Emery and Ikeda 1984; Prasad et al., 2002). The pair of the images could be co-registered within an error limit of one pixel (360 meters).

### **Cloud screening algorithm**

Sea water and its constituents alter spectral composition of visible light (400–700nm). Near infrared (NIR) radiation, however, is strongly absorbed by open ocean water. Clouds, in contrast, have a wide range of reflectivities at the wavelength measured by OCM sensor. Therefore, NIR radiation at 865 nm provides the best contrast between clear open ocean waters and clouds. An albedo-based cloud masking approach has been adopted for OCM processing in which the albedo at 865nm,  $a_{865}$  is calculated using the following equation:

$$a_{865} = \{L_t(865) / (t(865, h) L_i(865))\} \times 100\% \quad \dots\dots\dots(1)$$

where  $L_t(865)$  is the total radiance at the sensor at 865 nm,  $L_i(865)$  is the incident light at 865nm,  $t(865, h)$  is the diffuse transmittance between the surface and sensor at 865 nm, and  $h$  is the satellite zenith angle. For OCM data it was found that pixels at 865nm having albedo greater than 1.1% would be masked for clouds/thin clouds and haze. This threshold value is also found to be effective for masking land and sun glint affected pixels (SAC report, 2004).

### **Atmospheric and aerosol corrections**

The total signal received at the satellite altitude is dominated mostly by radiance contribution through the atmospheric scattering processes, and ~ 8 - 10% of the signal corresponds to oceanic reflectance. This necessitates corrections for the atmospheric effects. In a single scattering approach, the radiance received by a satellite sensor at the top of the atmosphere (TOA) in a spectral  $L_t(\lambda)$  comprises of the following components:

$$L_t(\lambda) = L_a(\lambda) + L_r(\lambda) + T(\lambda) L_g(\lambda) + t(\lambda) L_w(\lambda) \dots\dots (2)$$

where  $L_a$  and  $L_r$  are the radiance contributed by scattering in the atmosphere due to aerosol and Rayleigh scattering,  $L_g$  is the specular reflection (component of sun glitter) and  $L_w$  is water-leaving radiance.  $T$  and  $t$  correspond to direct and diffuse transmittance.

Because the OCM sensor has tilting mechanism to avoid sun glint (Mohan and Chauhan 2001), the effect of sun glitter is rather negligible. Since water-leaving radiance ( $L_w$ ) in 765 nm and 865nm bands is assumed to be equal to zero (Gordon and Clarke, 1981), TOA radiance in 765nm and 865 nm bands, as per equation (2) corresponds mainly to the contribution coming only from the atmospheric scattering. The equation (2) may, therefore, be written as:

$$L_t(\lambda) = L_a(\lambda) + L_r(\lambda) \text{ for } \lambda > 765 \text{ nm i.e. } L_w \neq 0 \dots\dots\dots(3)$$

In the equation (3) Rayleigh scattering  $L_r(\lambda)$  is computed from conventional and well-established theory as described in Chauhan et al. (2002 and references therein).  $L_a$  has been determined from the following relation:

$$L_a(\lambda) = L_t(\lambda) - L_r(\lambda) \text{ for } \lambda \leq 765 \text{ nm} \dots\dots\dots(4)$$

The 765 and 865nm channels of IRS-P-4 OCM (in NIR region) were used to obtain a relationship for spectral dependence of the aerosol optical depth on a pixel-by-pixel basis. Gordon and Wang (1994) had proposed an exponential relationship for spectral behavior of aerosol optical depth. An analysis of data on aerosol optical depth (AOD) collected during the satellite overpass had endorsed the exponential spectral dependence of the marine aerosols in the Arabian Sea (Chauhan et al. 2002) as well. It has been inferred that the exponential wavelength dependence was found to provide a better representation of the spectral decrease in the AOD than the conventionally accepted power law dependence for almost all the satellite overpass days for IRS P-4 data (Chauhan et al. 2002). We have therefore used an exponential function to estimate an epsilon value with 765 and 865nm bands for all cloud free pixels. The epsilon function ( $\epsilon$ ) was defined as:

$$\epsilon = L_a(765) / L_a(865) \dots\dots\dots (5)$$

After these corrections, water-leaving radiance in desired wavelengths was computed from the following relation:

$$L_w(\lambda < 750) = (L_{ac}(\lambda) - L_a(865) \exp\{\log(\epsilon) / (865 - 765)\} (865 - \lambda)) / t(\lambda) \dots\dots\dots (6)$$

where  $L_{ac}(\lambda)$  is the Rayleigh and ozone corrected radiances for  $\lambda < 750$  nm and  $t(\lambda)$  is diffuse transmittance.

After these corrections, TSM concentration has been derived from the following relations:

$$\text{Log}(S) = 1.83 + 1.26 \text{Log}(\chi S) \quad \forall 0.0 \leq S \leq 40.0 \dots\dots(7)$$

where S is particulate suspended matter ( $\text{mg l}^{-1}$ ) and  $\chi S$  is a variable defined as:

$$\chi S = [\text{Rrs}(555) + \text{Rrs}(670)] \times [\text{Rrs}(555) / \text{Rrs}(490)]^{0.5} \dots\dots(8)$$

where Rrs ( $\lambda$ ) is remote sensing reflectance in respective wavelengths ( $\lambda$ ). The reported retrieval accuracy of TSM from OCM data is  $\pm 15\%$  (SAC Report, 2004).

Weekly imageries were validated with 10-12 pass synchronous measurements (Fig. 2-4) made using local fishing crafts. We have prepared average seasonal TSM abundance for pre-monsoon (March-May) SWM (June-September) and the post SWM (October -February) seasons. Because of an intense cloud cover, we found few cloud free images during June – September of 2007. Because of this limitation, we have prepared a composite TSM distribution for June – September of 2007. In view of intense cloud cover, the images of the SWM have limitation for validation of each of the imagery. However, because of close similarity in the patterns of TSM distribution in the measured and the imagery derived patterns, a clear demarcation of highly turbid coastal waters with that of the deeper mid – outer shelf TSM waters (water depth > 35 m) could be made. In order to estimate advection pathways of TSM, currents were measured synchronously with TSM measurement using CONtrol current meter (accuracy  $\pm 5\%$ ) at 2m water depth at 12 stations. The measurement of currents was carried out at 2 m water depth to minimize the effects of any surface perturbation in the hydrography arising out of operation of several crafts in the study area.

## RESULTS

Seasonal spatial variations in measured and imagery derived TSM are presented in Figures 2-4. We found a good correlation between the imagery derived and the measured data ( $r = 0.89$ ,  $p=0.001$ ;  $N=36$ ; for the SWM;  $r=0.98$ ;  $p=0.001$ ;  $n=78$  for the pre and the post SWM seasons; Fig. 5). However, the imagery derived values were underestimated over the inner shelf (restricted to optimum detection limit of the algorithm) with respect to in situ measurements during the SWM, and this has influenced the correlation between the measured and the imagery derived data (Fig. 5).

An intense and persistent cloud cover during the entire SWM has curtailed our efforts to correlate all the field data with appropriate pixel values in available satellite imageries. We therefore acknowledge limitation in our algorithm in Case II waters during the SWM. A persistent cloud cover

has hindered our efforts to improve algorithm. Pending the development and availability of an improved algorithm, we consider remote sensing maps as a qualitative pattern, and rely mostly on synoptic pattern derived from the field data. However, during the cloud free seasons, there is good agreement between the imagery derived and the field data (Figs. 2-5). Based upon the field and the imagery derived data, we have deciphered two regional patterns in the shallow regions of the inner shelf. Associated with a large fluvial influx due to the existence of a network of the rivers, the entire inner shelf was highly and uniformly turbid ( $\geq 40 \text{ mg l}^{-1}$  in imageries; measured  $> 86 \text{ mg l}^{-1}$ ; Fig. 3; 5) for about 25 km during the prevalence of the SWM. The width of this zone, however, reduced considerably upon cessation of the SWM (Figs 2, 4). The deeper regions ( $> 40 \text{ m}$ ), in contrast, had low and similar TSM throughout the year, and no significant enhancement in the contents of TSM has been observed over the regions deeper than 35 m during the SWM season ( $12\text{-}24 \text{ mg l}^{-1}$  during the SWM;  $12\text{-}18 \text{ mg l}^{-1}$  during the rest of the year; Figs 2-4). Current vectors during the SWM and the post monsoon season are presented in Fig 6. Current magnitude is similar round the year ( $22\text{-}72 \text{ cm sec}^{-1}$ ) in the shallow waters ( $< 20 \text{ m}$ ). Their magnitude was marginally reduced in the deeper waters ( $21\text{-}52 \text{ cm sec}^{-1}$ ). However, the direction of currents was different.

Equatorwards currents prevailed during the SWM (July-August, 2007). Their direction reversed to polewards during the post monsoon (November-December, 2007). Such a trend is in conformity with the reported hydrography (Vinayachandran et al., 1999; Kumar et al., 2004 and references therein).

## DISCUSSION

The past studies from the Arabian Sea have hypothesized a dominant control of the SW monsoon climatology on the magnitude of TSM influx into the sea (Nair et al., 1989; Haake et al., 1993). As per the rain gauge data of the Karwar (a coastal town situated at the northern end), our study area receives about 80% rainfall ( $\sim 2700 \text{ mm}$ ; Chauhan et al. 2011) during the SWM. There are several small rivers debouching into the study area (Fig. 1). These rivers originate in the Western Ghats (elevation  $\sim 1900 \text{ m}$  above mean sea level), are short (60-153 km in length), and are sustained from the SWM precipitation (Raghvan and Chauhan, 2011). The hilly terrain and a short course of these rivers seem to support high supply of TSM from the hinterland into the sea. We, therefore, link higher TSM during the SWM season in the shallow coastal waters with a high fluvial supply (Fig. 3).

An elevated supply of TSM into the sea during the SWM is endorsed further from its manifold reduction in the shallow coastal waters upon the cessation of the SWM (Figs. 2, 4). However, beyond 25 km, despite optimum precipitation and a large fluvial yield, TSM contents were similar

during the SWM and pre and post monsoon seasons (Figs 2-4). We infer therefore that the quantity of TSM in the deeper regions of the Arabian Sea does not enhance during the SWM.

Besides land supply, water column biogeochemical processes sustaining marine productivity were linked also with the augmentation of flux of suspended particulate matter (Haake et al., 1993 and references therein). Sea bed sediments archive the contribution from water column as well as from bed load. Our inferences are supported further from the characteristics of sediments over the sea bed.

Earlier studies (Hashimi and Nair, 1981; Chauhan and Gujar, 1996; Vora et al., 1996) have reported relict, coarse, carbonate sediments over the entire mid - outer shelf (age 8.0-9.1 ka BP). These studies have found no clays and fine-silt size detritus over the mid-outer shelf. We infer, therefore, a poor subsurface flux over the entire deeper regions of the mid-outer shelf (Figs. 2-4) despite a high fluvial supply of TSM during the SWM (characterized by intense upwelling and high marine productivity; Naqvi et al., 2009). Because the age of the sediments over the outer – shelf is ~ 8.0- 9.1 ka BP (Vora et al., 1996), it may also be inferred that there is no significant deposition of modern detritus through bed – load over the deeper regions. Our results show high seasonality (high during the SWM and low during the non monsoon months) in TSM over the shallow coastal waters. This trend is not found, however, over the deeper waters of the outer shelf, in which there is no change in the TSM contents, and these waters are persistently TSM poor round the year (Figs 2-4). Derived from the spatial variability in TSM and from the characteristics of the sea bed sediments, we infer that high supply of TSM from the local rivers are not carried into the deeper regions of the Arabian Sea, nor there is any subsurface flux of TSM over the deeper regions of the shelf along the SE Arabian Sea. Because there is low TSM in the deeper regions during the SWM, we have examined the role of the current regime.

We have observed moderate – strong alongshore currents (equatorwards during the SWM and polewards during pre and post monsoon season; Fig 6) all year round in our study area. Such hydrography is in conformity with reported regional hydrography from this region (Kumar et al. 2004). Such a hydrography is favorable for along-shore advection of fine suspended matter discharged by the local rivers. Upwelling is also reported in the offshore regions of the study area during the SWM (Naqvi et al, 2009 and reference therein). These processes collectively or individually are not favorable for sustaining a large across – shelf advection of suspended matter. The observed seasonal pattern of TSM (with no significant across shelf plumes; Figs 2-4) in the imageries as well as in the field measurements, therefore suggest stronger control of hydrography of the region. We therefore surmise that higher supply of particulate matter alone is not a contributing

factor for enhancing supply of the particulate matter into the deeper waters, and hydrographic regime plays a dominant role in redistribution and sequestering of the sediments in the shallow regions along the precipitation dominant regime of the SE Arabian Sea. The observed large scale entrapment of fluvial influx may have series of implication for the coastal zone management strategies. There exists a major naval base and several large and small harbors in the region. Because of neo urbanization, the area is witnessing a large deforestation, which will aid in increasing yield and supply of terrigenous matter into sea. This may have implication for the increased siltation of the channels of the harbor besides contributing to the deterioration in the optical properties of the sea water, a crucial factor maintaining depth of euphotic zone and regulating sun-limitation marine primary productivity in this region.

### ACKNOWLEDGMENT

The work is supported by funding from the Space Application Center, and IGBP- ISRO, Ahmedabad. Authors thank Indian Coast Guard for valuable support during collection of sea truth data. OSC acknowledges Director NIO for support. BRR is thankful to Mangalore University.

### LITERATURE CITED

- Chauhan, O. S. and Gujar, A. R., (1996). *Surficial clay mineral distribution on the southwestern continental margin of India: evidence of input from the Bay of Bengal*. Cont Shelf Res, 16, 321-333, doi:10.1016/0278-4343(95)00015-S.
- Chauhan, P.; Mohan, M.; Sarangi, R.K.; Kumari, B.; Nayak, S., and Matondkar, S.G.P., (2002). *Surface chlorophyll a estimation in the Arabian Sea using IRS-P4 Ocean Color Monitor (OCM) satellite data*. Int. J. Remote Sens., 23(8), 1663-1676.
- Chauhan, O.S.; Jayakumar, S.; Menezes, A.A.A.; Rajawat, A.S., Nayak, S.R. (2006). *Anomalous inland influx of the River Indus, Gulf of Kachchh, India*. Mar. Geol.: 229(1), 91-100
- Chauhan, O. S.; Vogelsang, E.; Basavaiah, N., and Kader, U. S. A., (2010a). *Reconstruction of the variability of the southwest monsoon during the past 3 ka, from the continental margin of the southeastern Arabian Sea*. J Quaternary Sci., 25(5), 798–807. doi: 10.1002/jqs.1359.
- Chauhan, O. S., A. M. Dayal, N. Basavaiah, and U. S. A. Kader (2010 b), *Indian summer monsoon and winter hydrographic variations over past millennia resolved by clay sedimentation*, *Geochem. Geophys. Geosyst.*, 11, Q09009, doi:10.1029/2010GC003067.

- Chauhan, O. S., B. R. Raghavan, K. Singh, A. Rajawat, Ajay, U. S. A. Kader, and S. Nayak (2011) *Influence of orographically enhanced SW monsoon flux on coastal processes along the SE Arabian Sea* J. Geophys. Res., doi:10.1029/2011JC007454 ( published on line).
- Emery, W. J. and Ikeda M., (1984). *A comparison of geometric correction methods for AVHRR imagery*. Can. J. Remote Sensing , 10, 46-56.
- Gordon, H. R. and Clarke, G. L., 1981. *Clear water radiance for atmospheric correction of CZCS imagery*. App Optics., 20, 4157–4180.
- Gordon, H. R., and Wang, M., 1994, *Retrieval of water leaving radiance and aerosol optical thickness over the oceans with SeaWiFS: A preliminary algorithm*. Applied Optics,33, 443–452.
- Haake, B.; Ittekkot, V.; Rixen, T.; Ramaswamy, V.; Nair, R. R., and Curry, W. B., (1993). *Seasonality and inter-annual variability of particle-fluxes to the deep Arabian Sea*. Deep-Sea Res. Part-I, 40(7), 1323-1344, doi:10.1016/0967-0637(93)90114.
- Haake, B.; Rixen, T.; Reemtsma, T.; Ramaswamy, V., and Ittekkot, V., (1996). *Processes determining seasonality and interannual variability of settling particle fluxes to the deep Arabian Sea*, In: Ittekkot, V., Schafer, P., Honjo, S., Depetris, P. J., (Eds.), Particle flux in the ocean. John Wiley and Sons, Chichester, 57, pp. 251-270.
- Hashimi, N. H. and Nair, R. R., (1981). *Surficial sediments of the continental shelf off Karnataka*. J Geol soc Ind., 22, 266-273.
- Kumar, P. S.; Narvekar, J.; Kumar, A.; Shaji, C.; Anand, P.; Sabu, P.; Rijomon, G.; Josia, J.; Jayaraj, K. A.; Radhika, A., and Nair, K. K. C., (2004). *Intrusion of the Bay of Bengal water into the Arabian Sea during winter monsoon and associated chemical and biological response*. Geophys Res Lett., 31, L15304, doi:10.1029/2004GL020247.
- Legeckis, R. and Pitchard J., (1976). *Algorithm for correcting the AVHRR imagery for geometric distortions due to the Earth curvature, Earth rotation and spacecraft roll attitude errors*. NOAA Tech Memo, NESS 77.
- Levitus, S.; Burgett, R., and Boyer, T. P., (1994). *World Ocean Atlas: Salinity, NOAA Atlas*. NESDIS, 3, US Dept of Commerce, NOAA, pp. 99.
- Mohan, M.; Chauhan, P.; Mathur, A., And Dwivedi, R. M., (1998). *Atmospheric correction of MOS-B data using long wavelength and PCI approaches: IRS-P3 MOS validation experiment: Ocean Applications, SAC Report No. SAC/RESA/MWRD/IRSP3/SN/02/98*, pp.14-22.
- Mohan, M. and Chauhan, P., (2001). *Simulation for optimal payload tilt to avoid sunglint in IRS-P4 Ocean colour Monitor (OCM) data round the Indian subcontinent*. International Jour Remote Sensing., 22, 185–190.
- Nair, R. R.; Ittekkot, V.; Manganini, S. J.; Ramaswamy, V.; Haake, B.; Degens, E. T.; Desai, B. N., and Honjo, S., 1989. *Increased particle flux to the deep ocean related to monsoon*. Nature, 338, 749–751. doi:10.1038/338749a0.

Nair, T. M .B.; Ramaswamy, V.; Parthiban, G., and Shankar, R., 1999. *Factors controlling vertical fluxes of particles in the Arabian Sea*. J Geol Soc Ind., 54(4), 369-378.

Naqvi, S. W. A.; Naik, H.; Jayakumar, A.; Pratihary, A. K.; Narvenkar, G.; Kurian, S.; Agnihotri, R.; Shailaja, M, S., and Narvekar, P. V., (2009). *Seasonal anoxia over the western Indian continental shelf*. In: Wiggert, J.D., Hood, R. R., Naqvi, S. W. A., Brink, K. H., Smith, S. L., (Eds.), Indian Ocean biogeochemical processes and ecological variability. Geophysical Monograph Series, Washington, DC, USA, 185, pp. 333-345.

Prasad, J. R.; Rajawat, A. S.; Pradhan, Y.; Chauhan, O. S., and Nayak, S. R., (2002). *Retrieval of sea surface velocities using sequential ocean colour monitor (OCM) data*. Proceedings of Indian Academy of Science (Earth Planet Science), 11, 189–195.

Raghavan, B. R. and Chauhan, O. S., (2011). *Climate induced variability of suspended matter and nutrient in the discharge of Kali River, Central West Coast of India*. International Journal of Earth Science and Engineering, (In Press).

Rixen, T.; Ramaswamy, V.; Gaye, B.; Herunadi, B.; Maier-Reimer, E.; Bange, H. W., and Ittekkot, V., (2009). *Monsoonal and ENSO impact on particle fluxes and the biological pump in the Indian Ocean*. In: Wiggert, J.D., Hood, R. R., Naqvi, S. W. A., Brink, K. H., Smith S. L., (Eds.), Indian Ocean biogeochemical processes and ecological variability. Geophysical Monograph Series, Washington, DC, USA, 185, pp. 365-383.

SAC Technical Report, (2000). *Test and evaluation report on IRS-P4 OCM special product generation software*. Report No. IRS-P4/SAC/RESA/MWRD/TR/12/2000, p. 29

SAC Report, (2004). *Atmospheric corrections, bio-optical algorithm development and validation of IRS-P4 OCM data (IRS-P4 OCM Utilisation/SATCORE Project Report)*. Scientific Report No. SATCORE/SAC/RESA/MWRG/SC/ 01/02, Space Application Center, Ahmedabad, p. 98.

Tassan S., (1994). *Local algorithm using SeaWiFS data for retrieval of phytoplankton pigment, suspended sediments and yellow substances in coastal waters*. Applied Optics, 12,2369-2378.

United Nations Educational, Scientific, and Cultural Organization (UNESCO), (1994). *Protocols for the Joint Global Ocean Flux Study (JGOFS) Core Measurements, in Manual and Guides 29*, Paris, Scientific committee on oceanic research, pp. 170.

Vora, K. H.; Wagle, B. G.; Veerayya, M.; Almeida, F., and Karisiddaiah, S. M., (1996). *A 1300 km long late Pleistocene-Holocene shelf edge barrier reef system along the western continental shelf of India: occurrence and significance*. Mar Geol., 134, 145–162, doi:10.1016/0025-3227(96)00029-1.

Vinayachandran, P. N.; Masumoto, Y.; Mikawa, T., and Yamagata, T., 1999. *Intrusion of the southwest monsoon current into the Bay of Bengal*. J Geophys Res, 104(C5), 11077-11085, doi: 10.1029/1999JC900035.

Weaver, C. E., (1989). *Clays, Muds and Shales, in Developments in Sedimentology*, 44, Elsevier, Amsterdam.

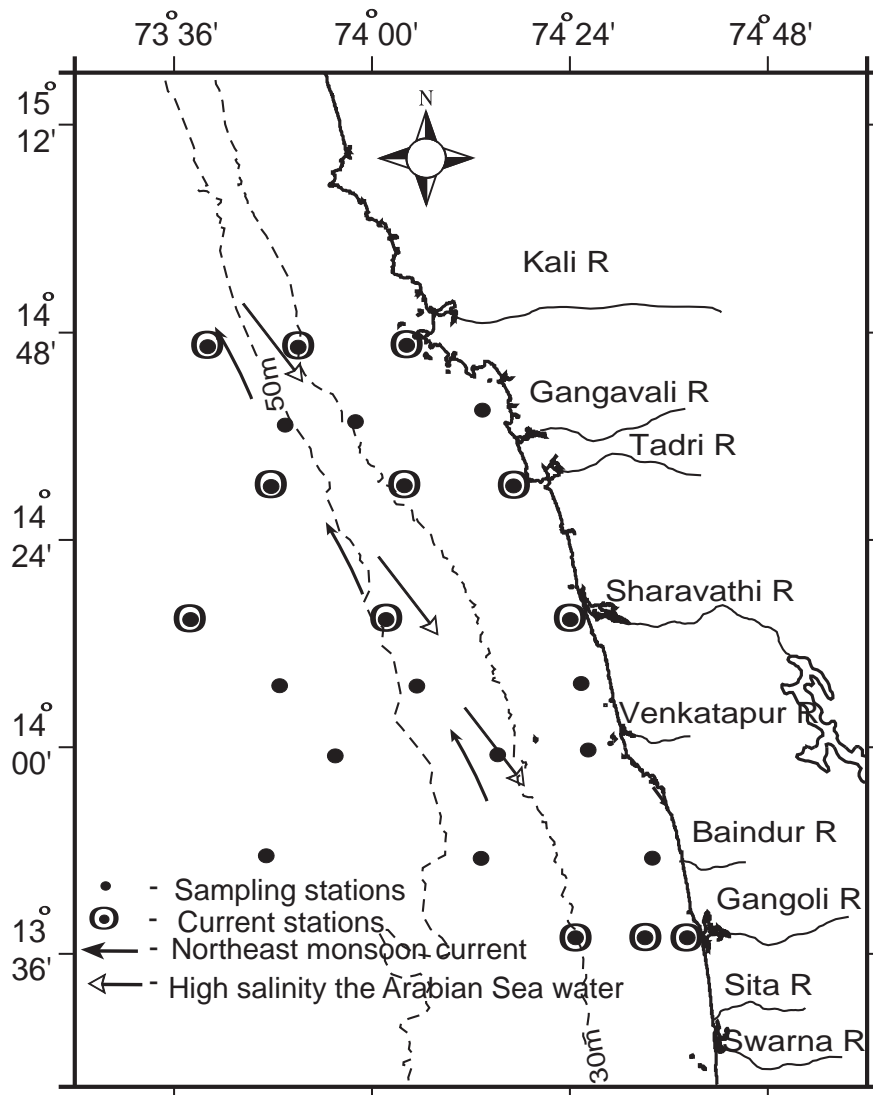


Fig 1: Study area together with location of stations along with prevalent hydrography. The local rivers debauching into the Arabian Sea are also shown.

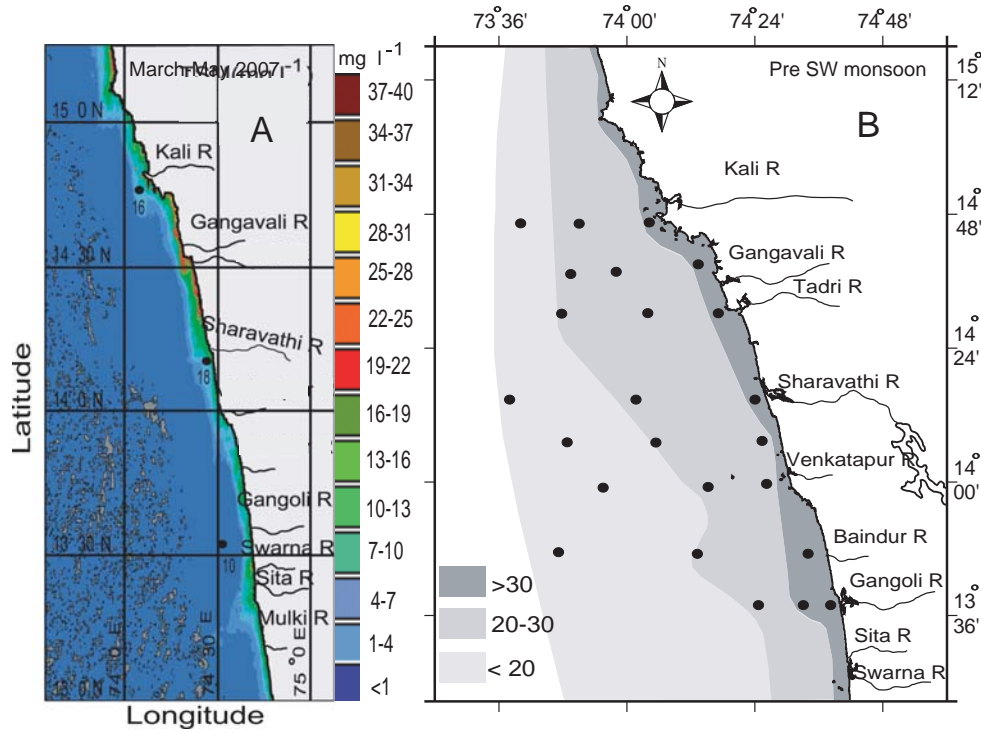


Fig 2: Validated, imagery derived (monthly averaged), synoptic patterns of TSM for March-May of 2007 (pre- monsoon season).

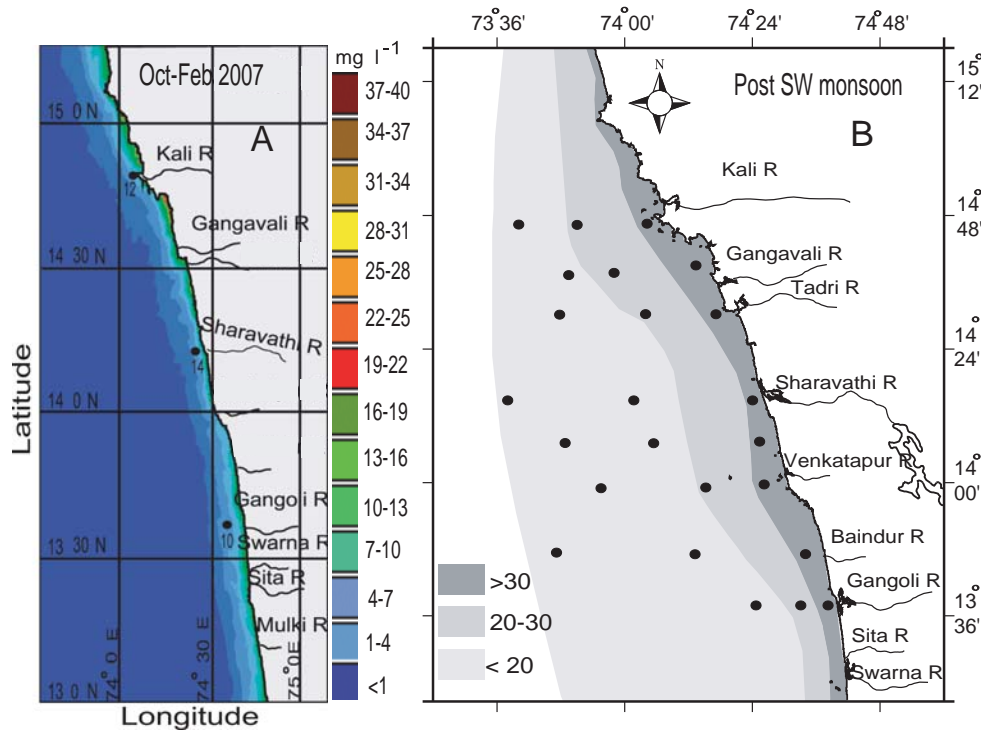


Fig 3: Measured and validated, imagery derived, monthly averaged synoptic patterns of TSM for June-September of 2007 (SWM season).

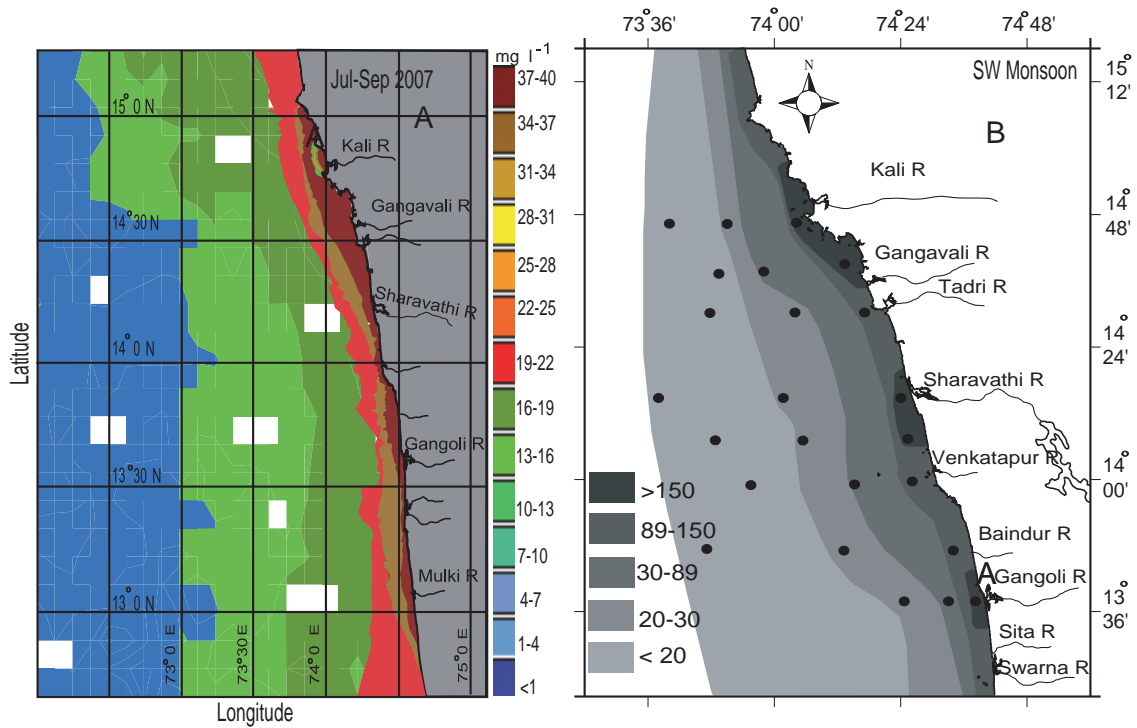


Fig 4: Same as Fig 2 but for October -February (post-monsoon) of 2007.

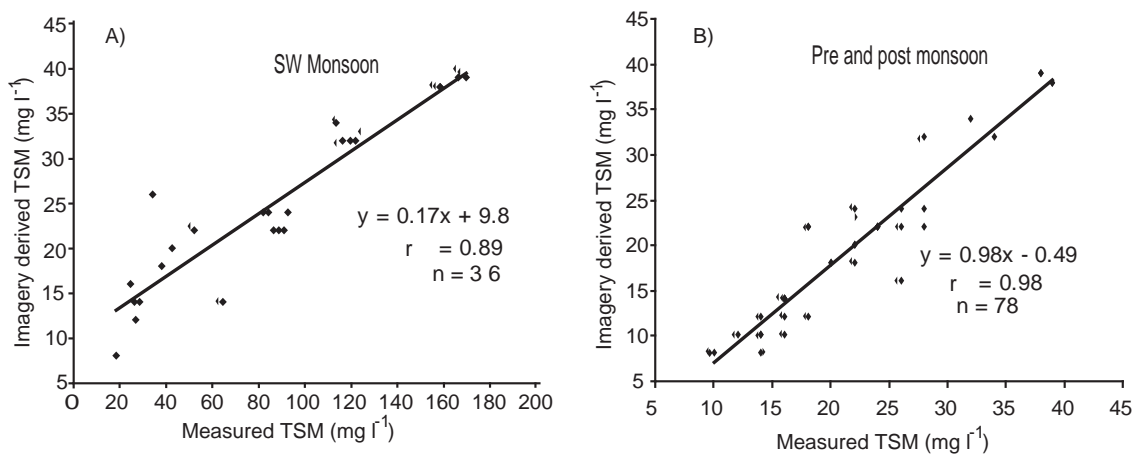


Fig 5: Measured current vectors in the study area during the SW monsoon (July-August) and the post monsoon season (October- November) of 2007.

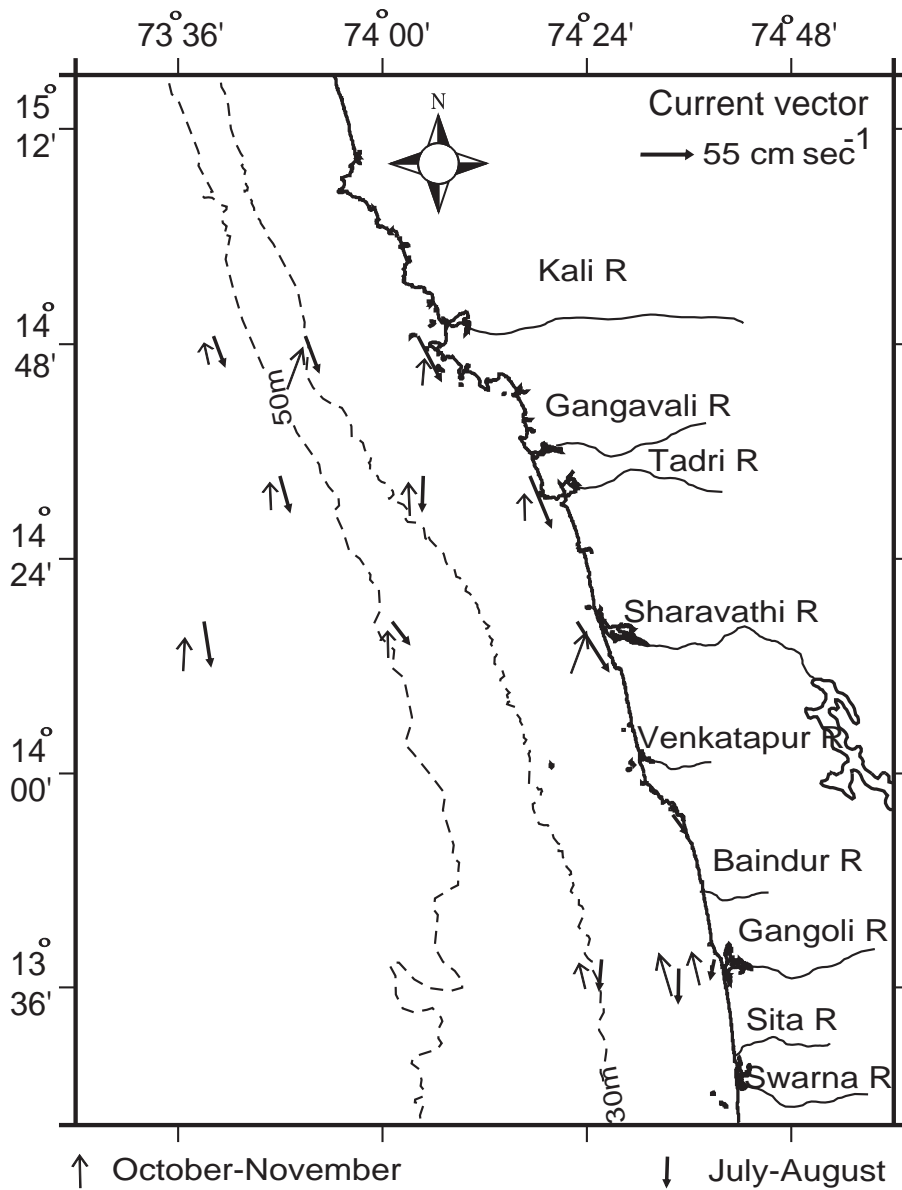


Fig 6: Measured current vectors in the study area during the SW monsoon (July-August) and the post monsoon season (October- November ) of 2007.